Pressure-Strain Correlations in Curved Wall Boundary Layers

S. K. Hong* and S.N.B. Murthy†
Purdue University, West Lafayette, Indiana

Pressure-strain correlations represent a redistribution of turbulence energy in shear flows and, therefore, are often included in modeling as some part of production and dissipation of Reynolds stress. It is then of interest to establish what portion of the energy spectrum contributes to pressure-strain correlations. Considering wall-bounded flows, the correlations have been determined, utilizing the large-eddy interaction model (LEIM), for the cases of boundary-layer flows past convex, concave, and flat walls, the latter also in a case where the flat wall follows a convex wall. The LEIM also provides a means of determining the contribution from different parts of turbulence spectra to the correlations in different regions across the boundary layer.

Introduction

PRESSURE-STRAIN correlations present a problem in closure of describing equations for turbulent flows. Several models have been suggested in the literature.[1-7] Measurement is not entirely trustworthy in the body of flows. Corrsin and Kollman[8] had made an important and successful attempt at evolving a method of obtaining pressure-strain correlations by computational experimentation and demonstrated the applicability of the method in the case of uniform shear flow. In a discussion of Ref. 8, Bradshaw raised an interesting question concerning pressure-strain correlations, namely, what portion of the energy spectrum contributes to the pressure-strain correlations that is represented in modeling as some part of production and dissipation of Reynolds stresses.

The large-eddy interaction model (LEIM)[9-11] provides a framework for the determination of the contribution by a wavenumber range of spectra to various turbulence-related quantities including the pressure-strain correlations. Within that framework the pressure-strain correlations are expressed in terms of large-eddy spectra that are obtained by solving dynamical equations for large eddies. The equations describe interactions of large eddies with mean flow and all of the eddies in the mixed (x,k) space where x space corresponds to coordinate(s) containing inhomogeneity of turbulence and k is the wavenumber space. The LEIM thus not only permits a determination of the contribution of different parts of the turbulence spectrum to any chosen turbulence process parameter, but also provides a means of testing the validity of any model that may be developed for the parameter under consideration.

When an incompressible, wall boundary layer is subjected to an additional strain such as curvature, there arises a special opportunity (based also on practical needs) for establishing and explaining the changes in the relative contribution of different parts of the spectrum to pressure-strain correlations compared to the flat-plate case and for determining the applicability and implications of current models. Thus, it can be shown that for different types of curvatures and curvature-relaxation situations, different parts of the spectrum make appreciably nonuniform contributions in different spatial directions and in different parts of the boundary layer, although in all cases the contribution of energetic eddies is substantial.

Large-Eddy Interaction Model

Framework

The large-eddy interaction model (LEIM) has been shown to be a useful framework in assessing the nature of turbulent transport, in particular for variously curved wall boundary-layer flows.[9-11] The LEIM is in essence based on the following formulation.

The velocity fluctuations u_i are decomposed into orthonormal functions $\phi_i^{(n)}$, that is,

$$u_i(x,t) = \sum_{n=1}^{\infty} \alpha_n \phi_i^{(n)}(x,t) \tag{1}$$

where α_n are random coefficients and $\phi_i^{(n)}$ deterministic orthonormal functions satisfying[12]

$$\overline{\alpha_m^* \alpha_n} = \lambda^{(n)} \delta_{mn}$$

$$\int \phi_i^{(p)}(x,t) \phi_i^{(q)*}(x,t) \mathrm{d}x\mathrm{d}t = \delta_{pq}$$

where $(\ )^*$ denotes the complex conjugate and $\lambda^{(n)}$ the turbulent kinetic energy of the whole flowfield associated with the $\phi_i^{(n)}$ mode. For the first mode $\phi_i^{(1)}$, which is identified with large eddies[12] and is found to be most dominant over all other modes,[13,14] the dynamical equation becomes, under incompressible flow assumptions,

$$\frac{\partial \phi_i^{(1)}}{\partial t} + U_j \frac{\partial \phi_i^{(1)}}{\partial x_j} + \frac{\partial U_i}{\partial x_j} \phi_j^{(1)} + \frac{\partial}{\partial x_j} \left(\sum_{p=1}^{\infty} \sum_{q=1}^{\infty} \frac{\overline{\alpha_1^* \alpha_p \alpha_q}}{\lambda^{(1)}} \phi_i^{(p)} \phi_j^{(q)} \right) = \frac{\partial \pi^{(1)}}{\partial x_i} + \nu \frac{\partial^2 \phi_i^{(1)}}{\partial x_j^2} \tag{2}$$

where

$$\lambda^{(1)} \equiv \overline{\alpha_1 \alpha_1^*}, \quad \pi^{(1)} \equiv -\frac{1}{\rho} \frac{\overline{\alpha_1^* p}}{\lambda^{(1)}}$$

The indices i, $j = 1, 2, 3$ represent the streamwise direction x, the local normal to the wall y, and the spanwise direction z, respectively. For the pressure fluctuation $\pi^{(1)}$, one can obtain

Presented as Paper 84-1671 at the AIAA 17th Fluid Dynamics, Plasmadynamics, and Lasers Conference, Snowmass, CO, June 25-27, 1984; received April 15, 1985; revision received Sept. 27, 1985.

*Research Assistant, School of Aeronautics and Astronautics; presently, Visiting Assistant Professor, Department of Mathematics, University of Texas at Arlington. Member AIAA.

†Senior Researcher, School of Mechanical Engineering. Member AIAA.

the Poisson equation imposing the continuity relation; thus,

$$\frac{\partial^2 \pi^{(1)}}{\partial x_j^2} = 2\frac{\partial U_j}{\partial x_k}\frac{\partial \phi_k^{(1)}}{\partial x_j} + \frac{\partial^2}{\partial x_k \partial x_j}\left(\sum_{p=1}^{\infty}\sum_{q=1}^{\infty}\frac{\overline{\alpha_1^*\alpha_p\alpha_q}}{\lambda^{(1)}}\phi_j^{(q)}\phi_k^{(p)}\right) \tag{3}$$

The nonlinear eddy-eddy interaction terms in Eqs. (2) and (3) representing transport of self-interactions of various sizes of eddies may, in general, be expressed in terms of the local value for the large eddy $\phi_i^{(1)}$ and of its subsequent derivatives, $\partial\phi_i^{(1)}/\partial x_j$, $\partial^2\phi_i^{(1)}/\partial x_j^2$,.... Two specific formulations have been considered in the use of LEIM. In one case,[9] a gradient diffusion model has been utilized as

$$-\sum_{p=1}^{\infty}\sum_{q=1}^{\infty}\frac{\overline{\alpha_1^*\alpha_p\alpha_q}}{\lambda^{(1)}}\phi_i^{(p)}\phi_j^{(q)} = \epsilon_{ik}\frac{\partial \phi_k^{(1)}}{\partial x_j} + \epsilon_{jk}\frac{\partial \phi_k^{(1)}}{\partial x_i} \tag{4}$$

where ϵ_{ij} is a second-order anisotropic eddy viscosity. Further, ϵ_{ij} is related to mean shear for boundary-layer flows,

$$\epsilon_{ij} = (C_i \ell)^2 \frac{\partial U}{\partial y}\delta_{ij}$$

where C_i are transport coefficients and ℓ the integral scale proportional to the Prandtl mixing length scale. As an alternative to the gradient diffusion hypothesis [Eq. (4)], a transport hypothesis based on a finite velocity scale has been considered[11] in the following form:

$$-\sum_{p=1}^{\infty}\sum_{q=1}^{\infty}\frac{\overline{\alpha_1^*\alpha_p\alpha_q}}{\lambda^{(1)}}\phi_i^{(p)}\phi_j^{(q)} = v_{ij}\phi_j^{(1)} + v_{ji}\phi_i^{(1)} \tag{5}$$

It may be pointed out that $\phi_i^{(1)}$ is only a first-order tensor quantity, yielding $\phi_{kj}^{(1)} = \phi_k^{(1)}\cdot\delta_{kj}$, hence, the indicated indexing.

Various turbulence structural quantities have been obtained (and reported[9-11]) for flat and curved walls utilizing the two hypotheses. Some aspects of the legitimacy and limitations of the two models have been discussed in Ref. 10. Here, gradient diffusion-based transport has been assumed in order to close the equations. The predictions obtained for pressure-strain correlations are not expected to be greatly affected by the assumption, since the anisotropic eddy viscosity values have been chosen such that the Reynolds stress and turbulence intensities are predicted correctly in relation to the experimental results.

In the case of a complex turbulent boundary layer such as that subjected to strain by wall curvature, it has been found necessary to consider the boundary layer in terms of three layers: the outer and inner layers and the viscous sublayer. Equations (2) and (3), therefore, are written to third order of the approximations (utilizing u_*/U_0, where parameter u_* is the wall-friction velocity) for each of the three regions. The equations, omitted here for brevity, can be found in Ref. 10.

Formulation

In any turbulent shear flow where mean velocities are two-dimensional (U, V, 0), such as in singly curved walls flows, a Fourier transform is applicable to the spanwise direction z. Considering time-averaged structure, the spectral functions may then be defined as

$$\hat{\phi}_i(x,y,k_3) = \frac{1}{2\pi}\int_{-\infty}^{\infty}\phi_i^{(1)}(x,y,z)\exp(-\hat{i}k_3 z)\mathrm{d}z \tag{6}$$

$$\hat{\pi}(x,y,k_3) = \frac{1}{2\pi}\int_{-\infty}^{\infty}\pi^{(1)}(x,y,z)\exp(-\hat{i}k_3 z)\mathrm{d}z \tag{7}$$

where $\hat{i} \equiv \sqrt{-1}$ and k_3 is the one-dimensional wavenumber. Introducing the above transforms into Eqs. (2) and (3) and dividing the resulting complex equations into real and imaginary parts, one obtains two sets of equations: one for (P_1, P_3, P_6, P_7) and a second for (P_2, P_4, P_5, P_8), where the following are introduced:

$$\hat{\phi}_1 = P_1 + \hat{i}P_2, \qquad \hat{\phi}_2 = P_3 + \hat{i}P_4$$
$$\hat{\phi}_3 = P_5 + \hat{i}P_6, \qquad \hat{\pi} = P_7 + \hat{i}P_8 \tag{8}$$

Here, real parts P_1, P_3, P_5, and P_7 are even functions and imaginary parts P_2, P_4, P_6, and P_8 are odd functions with respect to the wavenumber coordinate k_3. The two sets of equations can be found in Ref. 10. Although it may appear that it is necessary to solve both sets of equations, only the group of equations for P_2, P_4, P_5, and P_8 is selected for further analysis based on the following analytical and physical considerations. Analytically, the difference between the two groups of equations arise only in the sign of certain small terms that represent parts of eddy-eddy interactions or transport. Physically, if the large eddies are treated as long cylindrical structures (Ref. 15, p. 247) for wall shear flows, the large-eddy velocity components u and v can be represented by odd functions and the component w by an even function, which is consistent with the choice of the group of equations for P_2, P_4, P_5, and P_8. Various structural quantities can then be obtained[9-11] from the three normal stresses related, through Eqs. (6) and (7), to large-eddy spectra as follows:

$$\overline{u_i^2}(x,y) = \lambda^{(1)}\int_{-\infty}^{\infty}\hat{\phi}_i(k_3)\hat{\phi}_i^*(k_3)\mathrm{d}k_3 \tag{9}$$

It may be observed that $\lambda^{(1)}$ is to be understood as an average value (of turbulent kinetic energy) over k_3.

Pressure-Strain Correlation

Denoting the pressure-strain correlation term appearing in the Reynolds stress equation for $\overline{u_iu_j}$ by π_{ij},

$$\pi_{ij} = \frac{p}{\rho}\left(\frac{\partial u_i}{\partial x_j} + \frac{\partial u_j}{\partial x_i}\right) \tag{10}$$

and substituting the orthogonal expansion for the velocity fluctuation as given in Eq. (1) into Eq. (10), one obtains the following to first mode approximation:

$$\pi_{ij} \cong -\lambda^{(1)}\pi^{(1)}s_{ij}^{(1)} \tag{11}$$

where $s_{ij}^{(1)} \equiv \partial\phi_i^{(1)}/\partial x_j + \partial\phi_j^{(1)}/\partial x_i$ is the fluctuating rate of strain. Further, in terms of the spectrum for two-point pressure-strain correlation,

$$\hat{\pi}_{ij}(x,y,k_3) = \frac{1}{2\pi}\int_{-\infty}^{\infty}\pi_{ij}(x,y,r_3)\exp(-\hat{i}k_3 r_3)\mathrm{d}r_3 \tag{12}$$

or, inversely

$$\pi_{ij}(x,y,r_3) = \int_{-\infty}^{\infty}\hat{\pi}_{ij}(x,y,k_3)\exp(\hat{i}k_3 r_3)\mathrm{d}k_3 \tag{13}$$

where r_3 is the separation distance in the homogeneous space between the pressure fluctuation and the strain rate. It can be shown then that the spectrum for two-point pressure-strain correlation becomes related to the spectra for pressure fluctuation and the strain rate as

$$\hat{\pi}_{ij}^*(k_3) = -\lambda^{(1)}\hat{\pi}(k_3)\hat{s}_{ij}^*(k_3) \tag{14}$$

or,

$$\hat{\pi}_{ij}(-k_3) = -\lambda^{(1)}\hat{\pi}(k_3)\hat{s}_{ij}(-k_3) \tag{15}$$

where

$$\hat{s}_{ij}(x,y,k_3)=\frac{1}{2\pi}\int_{-\infty}^{\infty} s_{ij}^{(1)}(x,y,z)\exp(-\hat{i}k_3 z)\mathrm{d}z$$

When $r_3=0$, the two-point pressure-strain correlation reduces to the one-point correlation and Eq. (13) reduces to

$$\pi_{ij}(x,y)=\int_{-\infty}^{\infty}\hat{\pi}_{ij}(x,y,k_3)\mathrm{d}k_3 \tag{16}$$

or

$$\pi_{ij}(x,y)=-\lambda^{(1)}\int_{-\infty}^{\infty}\hat{\pi}(x,y,k_3)\hat{s}_{ij}^{*}(x,y,k_3)\mathrm{d}k_3 \tag{17}$$

Decomposition of the integrand in Eq. (17) into real and imaginary parts using Eq. (8) yields explicit expressions for π_{ij} as

$$\pi_{11}=-4\lambda^{(1)}\int_0^{\infty}P_8\left(\frac{\partial P_2}{\partial x}+\frac{P_4}{R}\right)\mathrm{d}k_3 \tag{18}$$

$$\pi_{22}=-4\lambda^{(1)}\int_0^{\infty}P_8\frac{\partial P_4}{\partial y}\mathrm{d}k_3 \tag{19}$$

$$\pi_{12}=-2\lambda^{(1)}\int_0^{\infty}P_8\left(\frac{\partial P_2}{\partial y}+\frac{\partial P_4}{\partial x}-\frac{P_2}{R}\right)\mathrm{d}k_3 \tag{20}$$

where R is the radius of wall curvature.

It may be appropriate to note here that Weinstock[16,17] has attempted analytical solutions for pressure-strain correlations in Fourier space. He has solved the fluctuating momentum equation for velocity spectrum and the Poisson equation for the pressure spectrum in the case of homogeneous flow. The spectra for velocity fluctuation and for pressure fluctuation are then substituted into an integral expression that is essentially the same as the one given in Eq. (17), thus obtaining a closed solution for the pressure-strain correlations. In contrast to his approach, the velocity and pressure spectra are obtained here directly from solution of the P_2, P_4, P_5, and P_8 equations.

Pressure-Strain Correlations in Curved Flows

Rotta[1] originally suggested the pressure-strain correlation as the sum of a production-like term and a dissipation-like term. That model has been retained by most investigators to date. Several modifications and improvements have been attempted based on various rationalizations in Refs. 2-7. Among those, Lumley[5] has provided what is undoubtedly the most rational method of modeling—particularly for the dissipation term. In a complex flow, such as a curved wall boundary layer, it is unclear if there is a unique or even an acceptably proved way of modeling the pressure-strain correlation. As pointed out in Ref. 6, the simplest and generally "successful" way of modeling the term is to write

$$\pi_{ij}=-C_1\frac{\epsilon}{k}\left(\overline{u_iu_j}-\frac{2}{3}k\delta_{ij}\right)-C_2\left(P_{ij}-\frac{2}{3}P_{kk}\delta_{ij}\right) \tag{21}$$

where C_1 and C_2 are empirical coefficients with the value of 1.8 and 0.6, respectively, k the turbulent kinetic energy, and ϵ the rate of dissipation of k. Also,

$$P_{ij}\equiv-\overline{u_iu_k}\frac{\partial U_j}{\partial x_k}-\overline{u_ju_k}\frac{\partial U_i}{\partial x_k} \tag{22}$$

and P_{kk} is the sum of the three diagonal terms of P_{ij}. The model represented by Eqs. (21) and (22) is the one employed in the current investigation. Additional comments are made in the next section.

Test Cases

The following four cases have been chosen for analysis and comparison: flat plate,[18] strong convex wall,[19] strong concave wall,[20] and relaxing flow.[19] The relaxing flow case refers to a flow over a flat plate following straining over a convex wall. The flow conditions for the test cases are summarized in Table 1. Figure 1 shows the geometrical configuration of the four test cases.

Calculation Procedure

In order to predict π_{ij} utilizing Launder's model [Eq. (21)], it is necessary to have values for distributions of k, ϵ, u_iu_j, and P_{ij} at each station along a wall. Those distributions can be obtained from experimental data (mean flow and turbulence quantities) reported in each of the four test cases chosen. Hence the distribution of π_{ij} is obtained utilizing Eq. (21).

Next, the equations for P_2, P_4, P_5, and P_8 in the (x,y) plane are solved for a chosen value of k_3 in the inner and outer parts of a boundary layer utilizing the appropriate equations, as stated earlier in the section on formulation. An upwind differencing method has been employed to solve the equations. It has been found[9-11] by trial-and-error that eight equally spaced values in the logarithmic scale for k_3, in the range of $0.05\leq k\leq 10.0$ 1/cm, together are adequate for obtaining turbulence quantities within acceptable errors in comparison with experimental data.

In order to find the contribution of a particular portion of spectrum to pressure-strain correlations, Eq. (17) can be rewritten as

$$\pi_{ij}=-\lambda^{(1)}\int_a^b\hat{\pi}\hat{s}_{ij}^{*}\mathrm{d}k_3 \tag{23}$$

where a and b are the lower and upper limits of a spectrum of interest. However, the eigenvalue $\lambda^{(1)}$ associated with the first mode $\phi^{(1)}$ still remains unknown in current formulation. Therefore, the distributions of π_{ij} with respect to y/δ

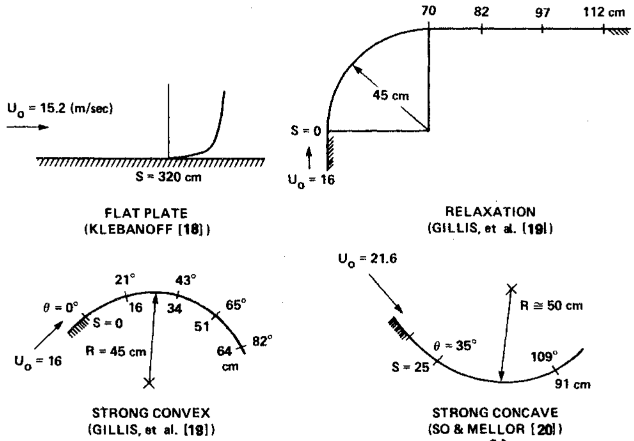

Fig. 1 Four test flow cases: distances s and angles θ are measured along the wall; freestream velocity is denoted by U_0.

Table 1 Flow conditions for the test cases

Cases	$C=1/R$, 1/m	U_0, m/s	θ_1, deg	δ_1, cm	θ_2, deg	δ_2, cm	Re, $\times 10^{-4}$
	Parameters						
Flat plate[18]	0.0	15.2	—	7.62	—	—	7.5
Strong convex[19]	2.22	16.0	20.0	3.86	80.0	4.49	4.0
Strong concave[20]	−2.0	21.6	35.0	3.30	109.0	5.60	4.7
Relaxing flow[19]	0.0	16.0	—	4.17	—	4.87	4.3

Note: Subscripts 1 and 2 denote the first and last measurement stations, respectively, along the wall. $Re=U_0\delta_1/\nu$.

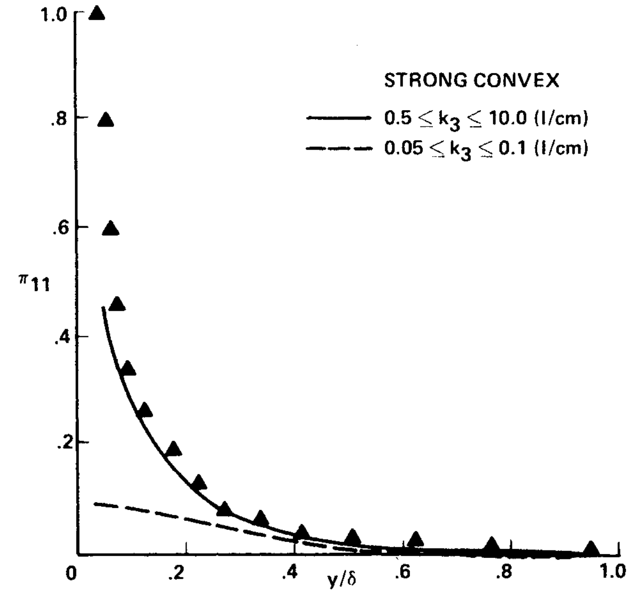

Fig. 2 Normalized distribution of pressure-strain correlation component π_{11} vs y/δ for the strong convex case[19] at $s=51$ cm (▲ Launder[6]).

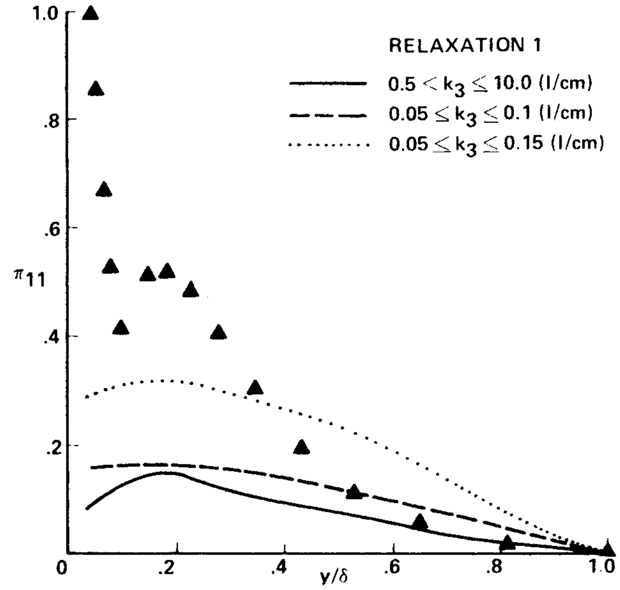

Fig. 4 Normalized distribution of pressure-strain correlation component π_{11} vs y/δ for the relaxing flow case[19] at $s=82$ cm (▲ Launder[6]).

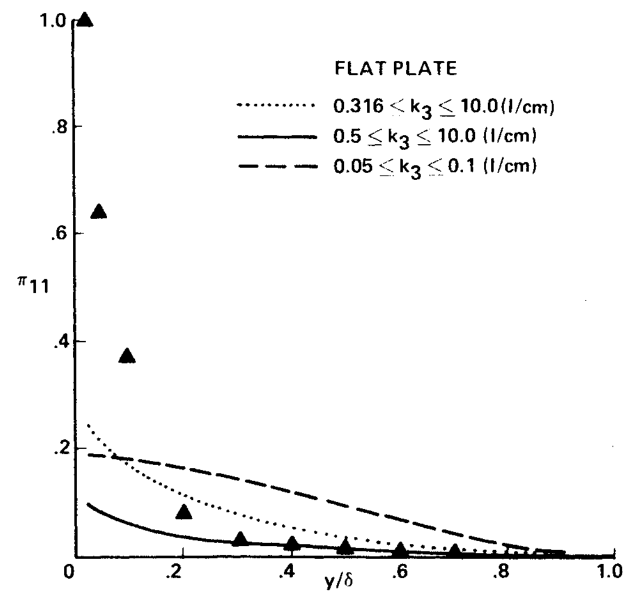

Fig. 3 Normalized distribution of pressure-strain correlation component π_{11} vs y/δ for the flat-plate case[18] (▲ Launder[6]).

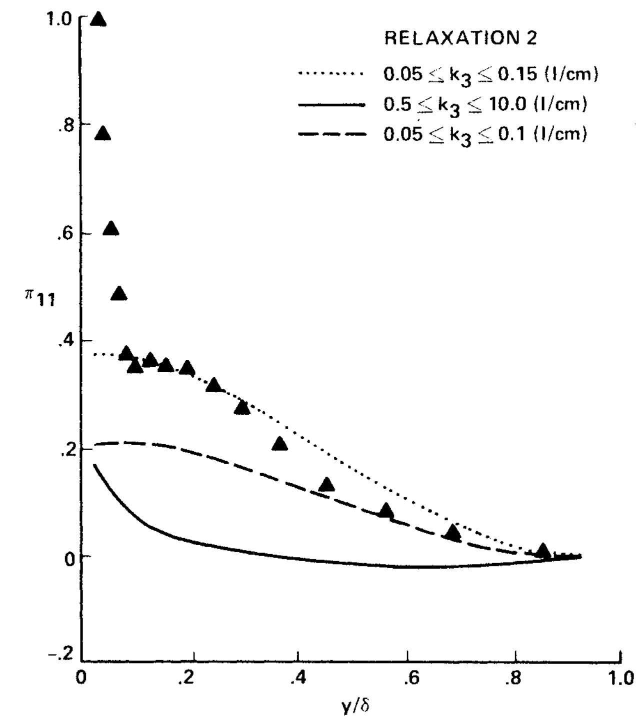

Fig. 5 Normalized distribution of pressure-strain correlation component π_{11} vs y/δ for the relaxing flow case[19] at $s=112$ cm (▲ Launder[6]).

(δ = boundary-layer thickness) are normalized by the maximum value at the station under consideration along the curved wall. The local maximum value is given by the expression

$$(\pi_{ij})_{\max} = -\lambda^{(1)} \int_{-\infty}^{\infty} \hat{\pi}(x, y_{\max}, k_3) \hat{s}_{ij}^{*}(x, y_{\max}, k_3) \mathrm{d}k_3 \tag{24}$$

where $y_{\max}$ is the value of y at which Launder's model [Eq. (21)] yields the maximum value for the available experimental data. In this manner, the pressure-strain correlations calculated utilizing Eqs. (23) and (24) yield the contribution from the chosen range of wavenumbers, $a \leq k_3 \leq b$, as a fraction of the correlation accounting for all of the spectrum.

Results and Discussion

The results of calculations for various flow cases are presented in Figs. 2-15. By heuristically connecting small wavenumbers to large eddies and large wavenumbers to small eddies, one can observe the following from the figures. In the figures, solid and variously broken lines represent the calculated results for π_{ij} obtained by use of Eq. (23) for various combinations of a and b and further divided by $(\pi_{ij})_{\max}$ [Eq. (24)]. The points marked by the symbol ▲ denote values obtained by use of Launder's model [Eq. (21)] and, once again, normalized by the maximum value in the boundary layer.

π_{11} Correlation

1) The contribution from large wavenumbers, namely, $k_3 \geq 0.5$ 1/cm, seems to yield reasonable π_{11} distributions in comparison with those based on Launder's model for convex flow case, as may be observed in Fig. 2. The value $k_3 = 0.5$

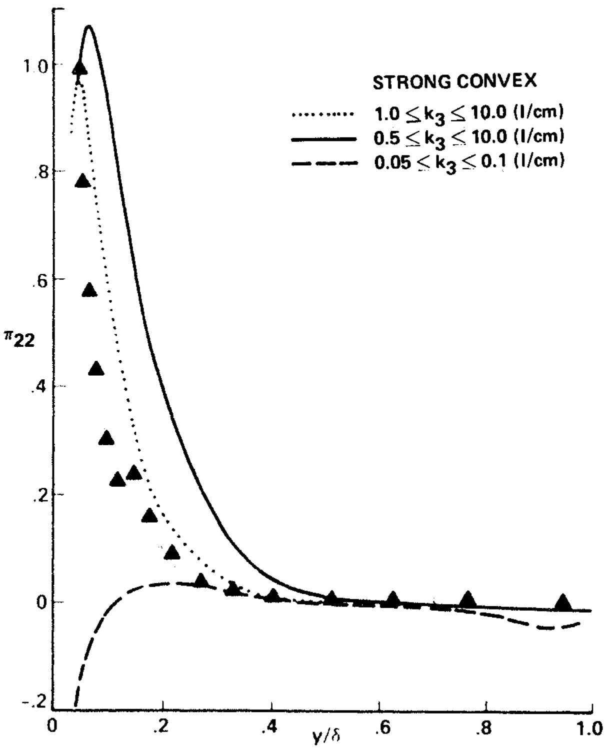

Fig. 6 Normalized distribution of pressure-strain correlation component π_{22} vs y/δ for the strong convex case[19] at $s=51$ cm (▲ Launder[6]).

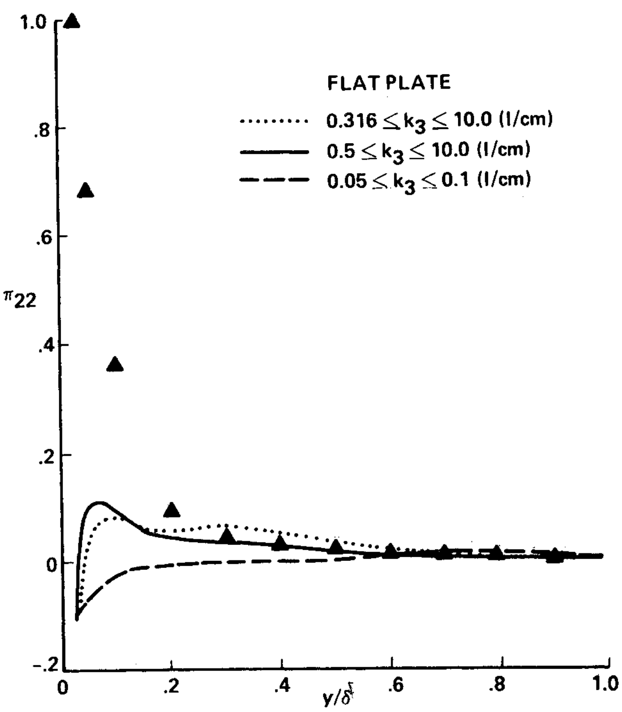

Fig. 7 Normalized distribution of pressure-strain correlation component π_{22} vs y/δ for the flat-plate case[18] (▲ Launder[6]).

l/cm coincides approximately with the one associated with energy-containing eddies.

2) In the flat-plate case (Fig. 3), a contribution from small wavenumber seems to be required in the inner part of the boundary layer in addition to that from the large wavenumber range, $k_3 \geq 0.5$ l/cm. It may be noted that the small wavenumber range is not associated with either the production part or the dissipation part of the pressure-strain correlation [Eq. (21)].

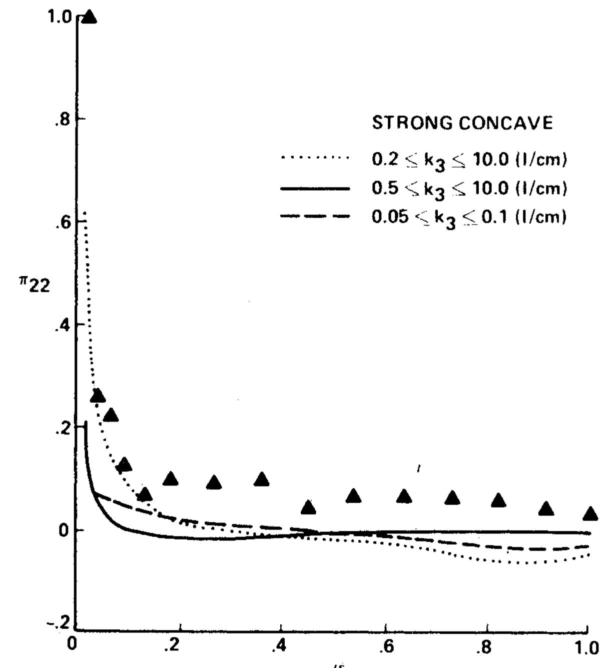

Fig. 8 Normalized distribution of pressure-strain correlation component π_{22} vs y/δ for the strong concave case[20] at $s=91$ cm (▲ Launder[6]).

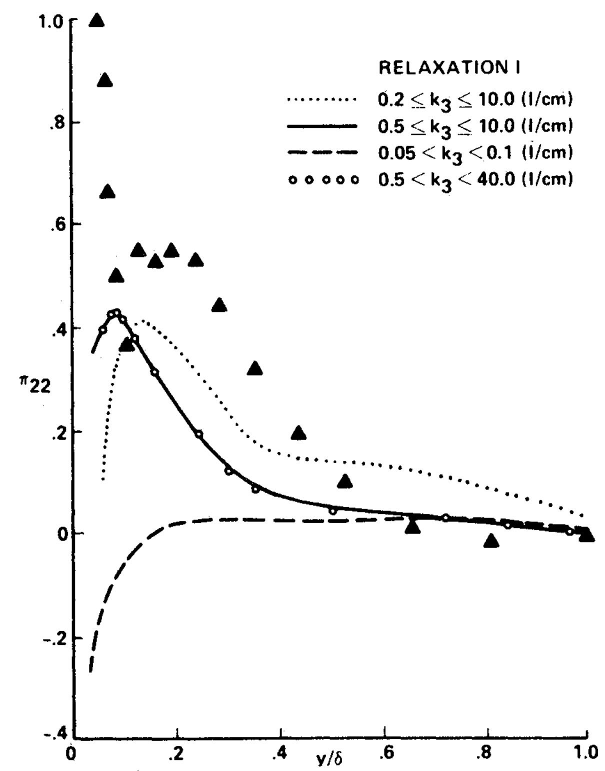

Fig. 9 Normalized distribution of pressure-strain correlation component π_{22} vs y/δ for the relaxing flow case[19] at $s=82$ cm (▲ Launder[6]).

3) Over the relaxation region shown in Figs. 4 and 5 ($s \equiv$ distance from origin of curved section = 82 and 112 cm, respectively) where large eddies can be seen to be severely affected by the sudden removal of curvature, the contribution from small wavenumbers becomes predominant across the entire boundary layer. This shows a difference in the role of large eddies in relaxing flow compared with that in cases 1

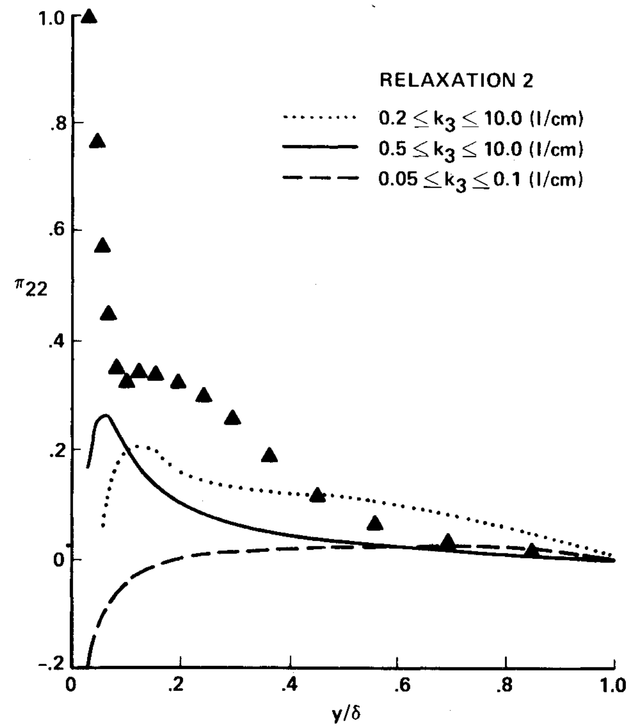

Fig. 10 Normalized distribution of pressure-strain correlation component π_{22} vs y/δ for the relaxing flow case[19] at $s=11$ cm (▲ Launder[6]).

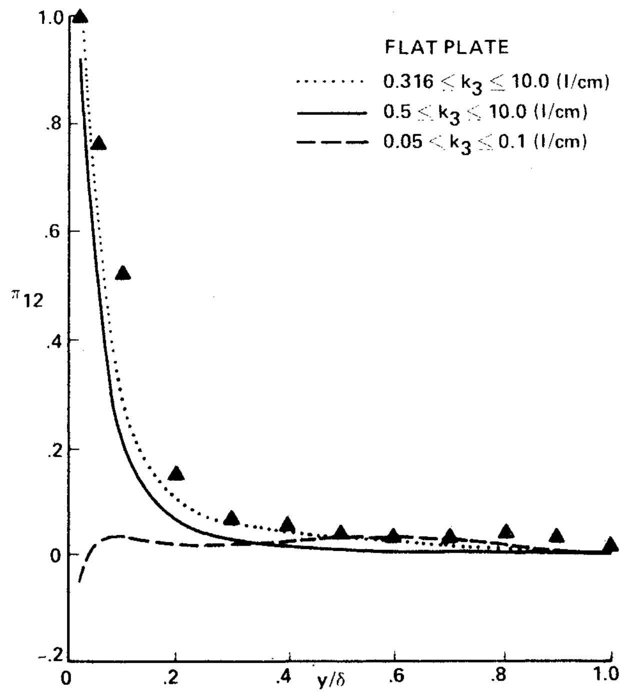

Fig. 12 Normalized distribution of pressure-strain correlation component π_{12} vs y/δ for the flat-plate case[18] (▲ Launder[6]).

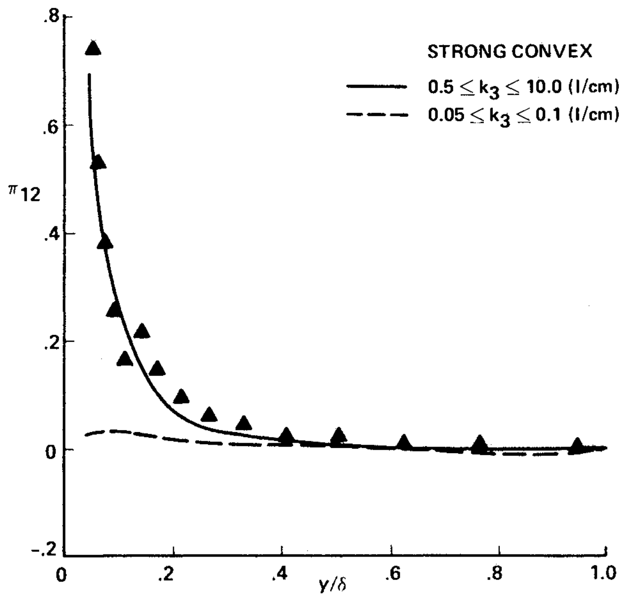

Fig. 11 Normalized distribution of pressure-strain correlation component π_{12} vs y/δ for the strong convex case[19] at $s=51$ cm (▲ Launder[6]).

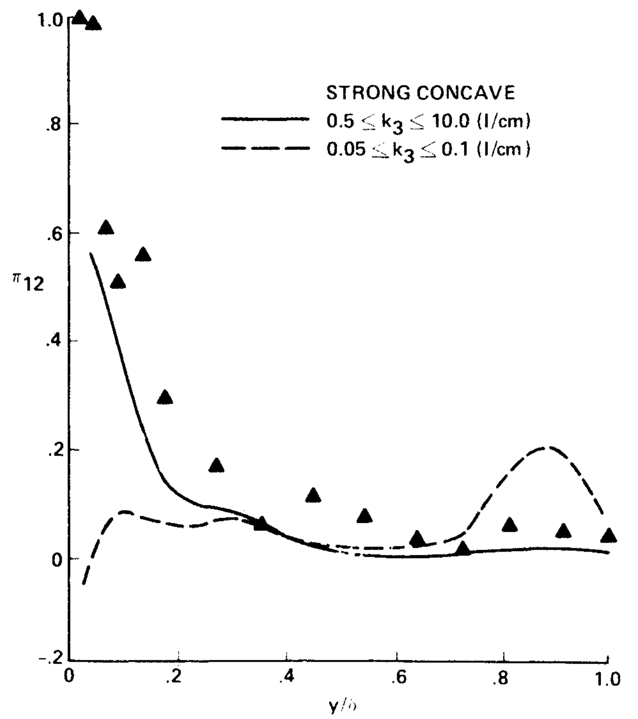

Fig. 13 Normalized distribution of pressure-strain correlation component π_{12} vs y/δ for the strong concave case[20] at $s=91$ cm (▲ Launder[6]).

and 2. This may even suggest that a third term is necessary in modeling the pressure-strain correlations [Eq. (21)] in order to include the significant contribution of the smallest wavenumber part of the spectrum for π_{11} component.

π_{22} Correlation

Turbulence quantities in the direction normal to the wall are of special interest in the case of curved wall flows in view of the radial pressure gradient introduced.

Contribution from large wavenumbers, $k_3 \geq 0.5$ 1/cm, again seems to follow trends similar to Launder's model. However, better agreement with Launder's model is obtained (Figs. 6-8) if the integration is carried out over slightly different wavenumber ranges, namely, $1.0 \leq k_3 \leq 10.0$ 1/cm for the convex wall, $0.5 \leq k_3 \leq 10.0$ 1/cm for the flat plate, and $0.2 \leq k_3 \leq 10.0$ 1/cm for the concave cases. Compared to the flat-plate case, the lower limit of integration seems to move toward a higher wavenumber for the convex curvature case (Fig. 6), where the large eddies become more anisotropic along the curved wall. In contrast, the lower limit of wavenumber tends to be smaller for the concave curvature case (Fig. 8), where large eddies tend to be isotropic. This is

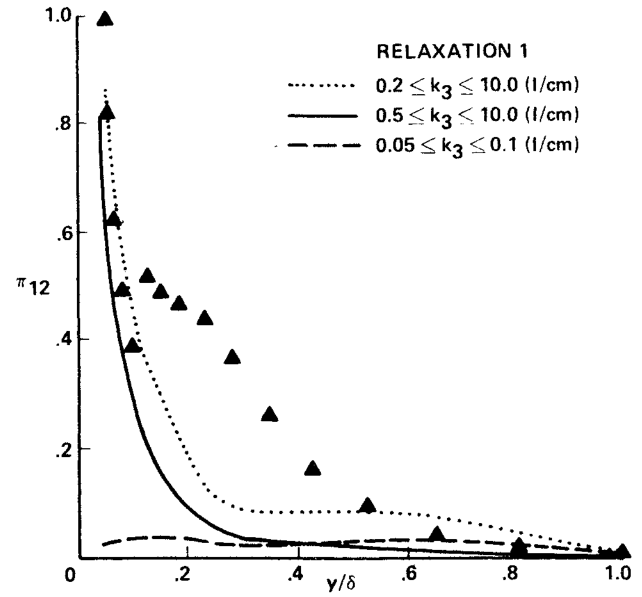

Fig. 14 Normalized distribution of pressure-strain correlation component π_{12} vs y/δ for the relaxing flow case[19] at $s = 82$ cm (▲ Launder[6]).

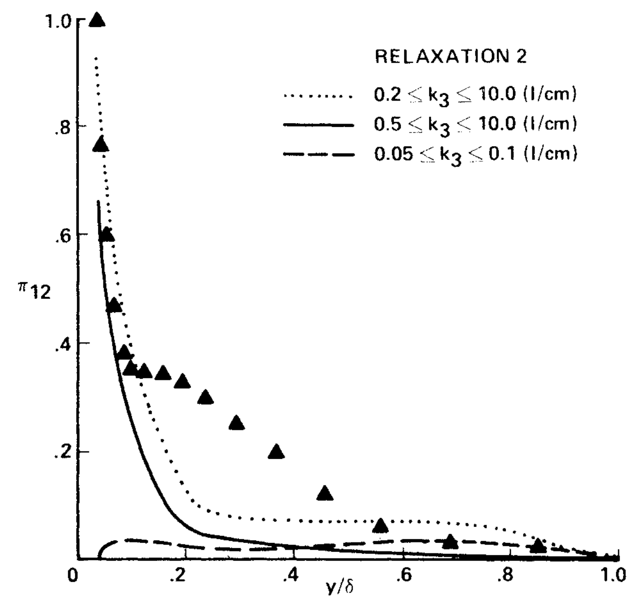

Fig. 15 Normalized distribution of pressure-strain correlation component π_{12} vs y/δ for the relaxing flow case[19] at $s = 112$ cm (▲ Launder[6]).

consistent with the experimental observation[21,22] that the introduction of wall curvature affects the v spectrum more than the u spectrum in the lowest portion of spectra.

The magnitude of π_{22} corresponding to large wavenumbers (solid line) decreases gradually with the wavenumber in the strong convex wall case (Fig. 6), the relaxation case (Figs. 9 and 10), and the flat-plate case (Fig. 7). Even after the flow has passed a distance of 10δ over the flat plate, the local pressure-strain correlation continues to be different from that obtained over a flat plate in the absence of initial strain.

When high wavenumbers (namely, $0.5 \leq k_3 \leq 40.0$ 1/cm) are included in Fig. 9 for π_{22}, the predicted result does not show a difference from π_{22} obtained for the range $0.5 \leq k_3 \leq 10.0$ 1/cm; this seems to indicate that; since they are the isotropic part of turbulence motion, small eddies do not influence the pressure-strain correlations.

π_{12} Correlation

Figures 11-15 suggest that the contribution from large wavenumbers ($k_3 \geq 0.5$ 1/cm) is adequate to match the calculated π_{12} correlation with the prediction based on Launder's model. Unlike π_{11}, the contribution of small wavenumbers to π_{12} is very small, even in the inner boundary region. This observation may be related to the fact that, since the dissipation term in the Reynolds shear stress equation is known to be small, the dissipation part of the pressure-strain term (π_{12}) should account for balancing the production of shear stress. As Bradshaw[23] has pointed out, the reason for the difference in behavior of π_{11} and π_{12} is most likely that "the u component in the inner layer has a large low-wavenumber 'inactive' component attributable to pressure fluctuation generated by the large eddies in the outer layer." Townsend[15] refers to those eddies as inactive because they are not associated with strong v motion and therefore contribute little to uv.

Conclusion

In summary, in flat and curved wall cases, large eddies, responsible for production of pressure-strain correlation, are dominant in the inner part of a boundary layer. Similarly, small eddies, responsible for dissipation, are dominant in the outer layer. However, the effect of small eddies in the outer part is greater than that of large eddies in the inner layer. In the case of a relaxing flow, the π_{11} component of the pressure-strain correlation is affected principally by large eddies that undergo adjustment continuously along the flat wall to the removal of curvature. This shows that during relaxation from curvature to flatness the inner part of the boundary layer and the large eddies affecting the production of π_{11} are the ones that undergo a slow change.

References

[1]Rotta, J. C., "Statistische Theorie Nichthomogener Turbulenz," *Zeitschrift für Physik*, Vol. 129, 1951, pp. 547-572.

[2]Launder, B. E., Reece, G. J., and Rodi, W., "Progress in the Development of a Reynolds Stress Turbulence Closure," *Journal of Fluid Mechanics*, Vol. 68, 1975, pp. 537-566.

[3]Mellor, G. L. and Herring, H. J., "A Survey of the Mean Turbulent Field Closure Models," *AIAA Journal*, Vol. 11, May 1973, pp. 590-599.

[4]Lumley, J. L. and Khajey-Nouri, B., "Computational Modelling of Turbulent Transport," *Advances in Geophysics*, Vol. 18, 1972, pp. 169-192.

[5]Lumley, J. L., "Computational Modeling of Turbulent Flows," *Advances in Applied Mechanics*, Vol. 18, 1978, pp. 77-123.

[6]Launder, B. E., "Reynolds Stress Closures—Status and Prospects," *Turbulent Boundary Layers—Experiments, Theory and Modelling*, AGARD CP 271, Jan. 1980, pp. 13.1-13.13.

[7]Launder, B. E. and Morse, A., "Numerical Prediction of Axisymmetric Free Shear Flows with a Reynolds Stress Closure," *Turbulent Shear Flows*, Vol. I, Springer-Verlag, New York, 1979, p. 307.

[8]Corrsin, S. and Kollmann, W., "Preliminary Report on Sheared Cellular Motion as a Qualitative Model of Homogeneous Turbulent Shear Flow," *Turbulence in Internal Flows*, edited by S.N.B. Murthy, Hemisphere Publishing Co., Washington, DC, 1977, pp. 11-33.

[9]Hong, S. K., and Murthy, S.N.B., "Structure of Turbulence in Curved Wall Boundary Layers," AIAA Paper 83-0457, Jan. 1983.

[10]Hong, S. K., "Large Eddy Interactions in Curved Wall Boundary Layers—Model and Implications," Ph.D. Thesis, Purdue University, West Lafayette, IN, Aug. 1983.

[11]Hong, S. K. and Murthy, S.N.B., "On Effective Velocity of Transport in Curved Wall Boundary Layers," *AIAA Journal*, Vol. 24, March 1986, pp. 361-369.

[12]Lumley, J. L., "The Structure of Inhomogeneous Flows," *Atmospheric Turbulence and Radio Wave Propgation*, edited by A. M. Yaglom and V. I. Tartarsky, Nauka, Moscow, 1967, pp. 166-177.

[13]Payne, F. R. and Lumley, J. L., "Large Eddy Structure of the Turbulent Wake Behind a Circular Cylinder," *The Physics of Fluids*, Vol. 10, 1967, pp. S194-S196.

[14]Lemmerman, L. A. and Payne, F. R., "Extraction of the Large Eddy Structure of a Turbulent Boundary Layer," AIAA Paper 77-717, June 1977.

[15]Townsend, A. A., *The Structure of Turbulent Shear Flow* (1st ed.), Cambridge, University Press, London, 1956.

[16]Weinstock, J., "Theory of Pressure-Strain-Rate Correlation for Reynolds-Stress Turbulence Closures, Part I: Off-Diagonal Element," *Journal of Fluid Mechanics*, Vol. 105, 1981, pp. 369-396.

[17]Weinstock, J., "Theory of Pressure-Strain Rate, Part 2. Diagonal Elements," *Journal of Fluid Mechanics*, Vol. 116, 1982, pp. 1-29.

[18]Klebanoff, P. S., "Characteristics of Turbulence in a Boundary Layer with Zero Pressure Gradient," NACA TN-3178, 1954.

[19]Gillis, J, C., Johnston, J. P., Moffat, R. J., and Kays, W. M., "Experimental Data and Model for the Turbulent Boundary Layer on a Convex, Curved Surface," NASA CR-3391, 1981.

[20]So, R.M.C. and Mellor, G. L., "An Experimental Investigation of Turbulent Boundary Layers Along Curved Surfaces," NASA CR-1940, 1972.

[21]Eskinazi, s. and Yeh, H., "An Investigation on Fully Developed Turbulent Flows in a Curved Channel," *Journal of the Aeronautical Sciences*, Vol. 23, Jan. 1956, pp. 23-34.

[22]Ramaprian, B. R. and Shivaprasad, B. G., "The Structure of Turbulent Boundary Layers Along Mildly Curved Surfaces," *Journal of Fluid Mechanics*, Vol. 85, 1978, pp. 273-303.

[23]Bradshaw, P., private communication, 1984.